IEEE Access
Multidisciplinary | Rapid Review | Open Access Journal

Received August 4, 2019, accepted August 26, 2019, date of publication August 28, 2019, date of current version September 12, 2019.

Digital Object Identifier 10.1109/ACCESS.2019.2938148

Voltage Waveform Transient Identification for Autonomous Load Coordination

SPENCER C. SHABSHAB[1], PETER A. LINDAHL[2], (Member, IEEE), J. KENDALL NOWOCIN[3], AND STEVEN B. LEEB[3], (Fellow, IEEE)

[1]Naval Nuclear Power School, U.S. Navy, Goose Creek, SC 29445, USA
[2]Exponent, Inc., Natick, MA 01760, USA
[3]Department of Electrical Engineering and Computer Science, Massachusetts Institute of Technology, Cambridge, MA 02139, USA

Corresponding author: Steven B. Leeb (sbleeb@mit.edu)

This work was supported in part by a Grant from The Grainger Foundation, and in part by an MIT Energy Initiative Cooperative Agreement with Exelon.

ABSTRACT Significant electrical loads such as HVAC systems can be made ''aware'' of the operation of other loads nearby in the electric grid. Local examination of the utility voltage waveform can provide this awareness without the need for a dedicated communication network. This is particularly true in low-inertia microgrids and ''soft'' sections of a utility network. This paper presents techniques for extracting frequency and voltage harmonic transients corresponding to individual load events. With data collected from a microgrid energized by diesel generators, we demonstrate the ability to identify the operation of HVAC units and generator dispatch events from their transient effects on the voltage using a cross-correlation based scoring algorithm. Ultimately, incorporating such awareness into load controllers allows loads to autonomously meet system-level objectives in addition to their individual requirements. For example, HVAC units could maintain occupant comfort while also reducing the utility's peak aggregate electrical demand by consuming electricity on a schedule interleaved with the operation of other nearby HVAC units.

INDEX TERMS Microgrids, smartgrids, autonomous systems, monitoring, load management, current-voltage characteristics, correlation, classification algorithms.

I. INTRODUCTION

Electric loads typically operate with uncoordinated schedules. For example, an environmental control unit (ECU) providing heating and cooling to a building (or section of a building) operates independently from other ECUs in neighboring buildings (or other sections of the building). The local temperature conditions determine the activation time for each ECU. ECU activation times can align, resulting in many ECUs operating simultaneously, with a maximum demand on the utility [1]. This schedule of operation is unfortunate and unnecessary. Generally, ECU operation could be interleaved to minimize peak demand while still maintaining occupant comfort. Many electric loads, including ECUs, could receive information to become ''aware'' of the operation of other loads [2]–[4]. This information could be exchanged through a dedicated wired network, radio-frequency communications, or power line communications [5], [6].

The associate editor coordinating the review of this article and approving it for publication was Dongbo Zhao.

Intriguing possibilities exist for the autonomous collection of operational information from neighboring loads through analysis of voltage measurements local to a load. Measurements of grid voltage have been used to track power quality [7], determine when emergency load shedding is required to maintain microgrid stability [8], and to detect microgrid islanding events [9]. This paper introduces new techniques for identifying load operation ''signatures'' strictly from measurements of utility voltage. These techniques are particularly applicable in low-inertia microgrids or ''street-level'' distribution networks where the utility may not be ''stiff,'' due to generator limitations or impedance from a local distribution transformer. Among other uses, this information could be used for autonomous control of cyclically operating loads [1], [10].

Techniques proposed here are demonstrated with voltage meter data [11] collected in the control panels of several ECUs at the U.S. Army's Base Camp Integration Laboratory (BCIL) at Fort Devens, MA. The BCIL is an archetypal forward operating base (FOB) with an islanded microgrid

powered by a bank of 60kW synchronous diesel generators under dispatch control [1], [10]. The responses of the line voltage to ECU turn-on/off events, generator dispatch/secure events (hereby referred to as generator turn-on/off events, respectively), and the turn-on/off events of other loads were observed under a variety of base load and generator configurations. Data collected for several days over a period of months showed good repeatability. This data was analyzed to extract operation signatures. A cross-correlation based transient identification technique presented here showcases the potential for algorithmic load event recognition using the extracted signatures.

II. SIGNATURE EXTRACTION FROM VOLTAGE

Relatively few references have looked at the recognition of voltage-only transient identification for nonintrusive monitoring. In [12], the authors present an analog front-end for examining voltage transients. This approach did not examine frequency variation on the utility as a potential data stream, and assumed frequency to be quasi-static over an estimation period. We demonstrate here that frequency variation and a direct digital examination of higher harmonics are both critical for effective transient identification in practical applications.

Relatively small grids or subsections of a larger grid are more likely to display voltage distortions, e.g., frequency deviations and harmonic content, that can be used as information for load control. Such distortions can be especially noticeable on islanded microgrids, where generation capacity and individual load demand may be comparable. This is the case at the BCIL, where the ECU heaters (10kW rating) consume approximately 17% of the rated power of a single 60kW diesel generator.

On such microgrids, electrical transients result in grid frequency deviations due to the finite bandwidth associated with synchronous generator field controllers and speed governors, as well as the frequency control of power electronic inverters connecting renewables or energy storage devices. These sources have finite output impedance and bandlimited control. They often exhibit load-dependent harmonic voltage distortion. This distortion is exacerbated by modern nonlinear loads demanding non-sinusoidal currents through the grid impedances [13]. Frequency and harmonic deviations also occur when generators come on-line or go off-line to match load demand. All of these deviations can serve as signatures to identify the load and generation status of the grid.

Frequency and harmonic distortions have been used previously as signatures for current-based nonintrusive load monitoring (NILM) [14]–[17]. Here, we propose a signal processing pipeline similar to the Sinefit spectral envelope preprocessor [17] originally designed for current-based NILM. The preprocessor employed here looks strictly at voltage waveforms, and includes signal processing modifications that improve harmonic extraction accuracy. Harmonic distortions in the voltage waveform can be small compared to harmonic content in current, and the new voltage waveform preprocessing algorithm discussed below provides critical resolution for identifying transients in the utility voltage waveform.

Fig. 1 depicts the signal processing pipeline for transient signature extraction. The processor takes a single-phase voltage, $v[n]$, sampled with frequency, f_s, and produces time-series "streams" of frequency estimates, $\hat{f}[m]$, and voltage harmonic coefficient estimates, $\hat{V}_k[m]$. Streams are provided at a sample rate double the line frequency, i.e., the rate of zero-crossings in the line voltage. From $v[n]$ the algorithm first locates voltage zero-crossings in time (ZCD module) by linearly interpolating between the voltage data points just before, $v\left[n_m^-\right]$, and just after, $v\left[n_m^+\right]$, the m^{th} zero crossing,

$$\hat{t}_z[m] = t\left[n_m^-\right] - \frac{v\left[n_m^-\right]}{f_s\left(v\left[n_m^+\right] - v\left[n_m^-\right]\right)}. \tag{1}$$

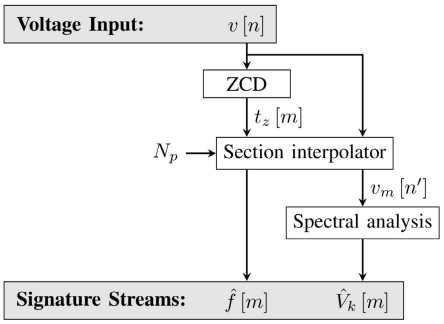

FIGURE 1. Signature extraction process from raw voltage measurements.

With this zero-crossing stream, the section interpolator module estimates the average frequency across the m^{th} data section of length N_p voltage periods as,

$$\hat{f}[m] = \frac{N_p}{\hat{t}_z\left[m + N_p\right] - \hat{t}_z\left[m - N_p\right]}. \tag{2}$$

The module then resamples the voltage waveform section at the rate,

$$f_s'[m] = \frac{N'[m]}{N_p}\hat{f}[m], \tag{3}$$

where

$$N'[m] = \left\lceil N_p \frac{f_s}{\hat{f}[m]} \right\rceil \tag{4}$$

is the number of new samples over the N_p period-length section. Here, $\lceil\cdot\rceil$ represents the ceiling function meaning that $N'[m]$ is the integer value larger than the "prorated" number of samples between voltage zero-crossings, $m - N_p$ and $m + N_p$. In this way, $f_s'[m]$ is the smallest sample rate higher than f_s that results in an exact integer number of samples in the data section. This process reduces the variance of the spectral leakage errors by aligning the frequency bins of the spectral analysis with the fundamental and harmonic

frequencies of interest. The coefficients for these components are calculated via the discrete Fourier Transform (DFT):

$$\hat{V}_k[m] = \sum_{n'=0}^{N'-1} v_m[n'] e^{-j2\pi kn'/N'}. \quad (5)$$

III. FIELD TESTING & OBSERVATIONS

To assess the potential for identifying microgrid events through voltage monitoring, measurements were taken at the BCIL during a series of ECU and generator turn-on and turn-off events on the microgrid illustrated in Fig. 2. During testing, either one or both of two 60kW diesel generators provided 120/208V, 60Hz service to the microgrid. The ECUs each provide heat to a section of a tent complex (Fig. 3). The ECUs receive power via radial connections from a common point of coupling with the generators. In addition to the ECUs, a three-phase variable-resistive load bank capable of adding base load from zero watts to approximately 25kW was connected to the grid in order to widen the base load variation during testing. Other camp loads, e.g., lighting, plug loads, and notably a latrine sewage pump, were present and operating. However, with the exception of the latrine pump, these lighting, plug load, and transformer loads draw much smaller transient currents than the ECUs and therefore did not create significant voltage transients.

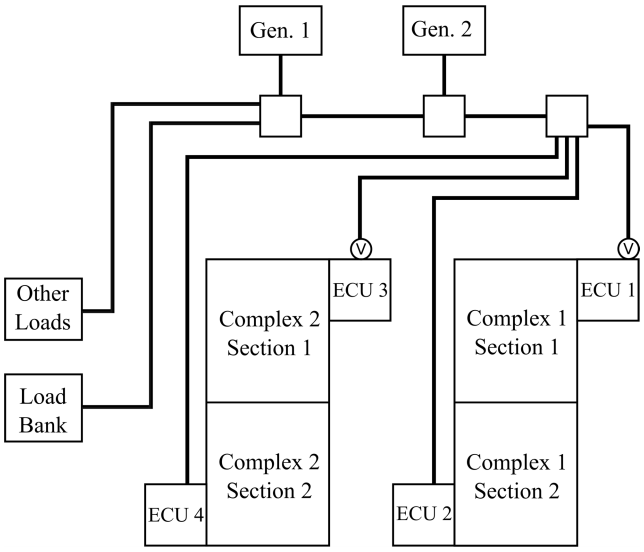

FIGURE 2. Test setup for voltage measurements at the BCIL. Voltage meters measuring at terminals of ECUs one and three are labeled "V".

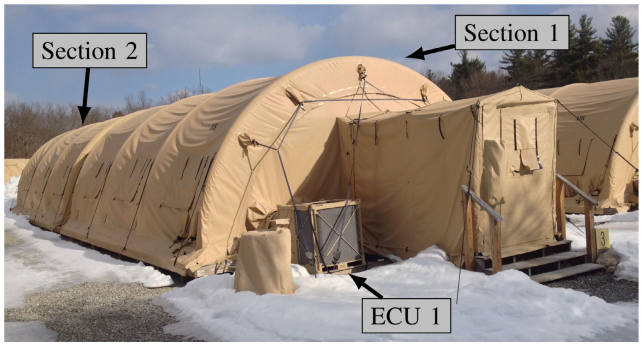

FIGURE 3. Tent complexes consist of two adjoined tents each with a dedicated ECU.

The response of the line voltage to ECU, latrine pump, and generator events was measured under a variety of base load and generator configurations. Generator events occurred according to their dispatch control rules. A second generator comes online after load demand exceeds 48kW (80% single generator capacity) for 10 consecutive seconds. This second generator will go offline after load demand drops below 36kW (60% single generator capacity) for five consecutive minutes. Over the course of testing, several hundred ECU turn-on/off transients, eight generator turn-on transients, seven generator turn-off transients, and four latrine pump turn-on transients were observed and analyzed for event signatures in the voltage waveform.

The voltage meters [11] installed in ECUs 1 and 3 sampled voltage at $f_s = 8$ kHz with 10-bit resolution. This data was analyzed over $N_p = 6$ period-length windows, a length we found to provide a good tradeoff between "smoothing" measurement and process noise and capturing frequency and harmonic features related to grid transients. This window of six periods has proven useful in practice, but it could be varied to tune performance of the voltage waveform estimator in different locations. Spectral analysis was performed for the fundamental and the 3^{rd}, 5^{th}, and 7^{th} harmonics, as these odd harmonics are often-present artifacts due to load current distortions [17] and generator or source harmonic distortion, e.g., from space harmonics in the magnetic field of a synchronous generator [18]. Other harmonics might be of interest for loads with richer high frequency harmonic current distortion and sources with different harmonic voltage signatures. Of these harmonic streams, the 7^{th} harmonic estimate, $\hat{V}_7[m]$, proved most useful at BCIL because of the harmonic content generated by the ECU loads and the harmonic signatures of the generators. At BCIL, an examination of seventh harmonic and also the frequency estimate stream, $\hat{f}[m]$, was sufficient for identifying all major electrical events.

IV. EVENT TRANSIENT SIGNATURES

Field testing revealed that the voltage transients induced by electrical events vary in character. The details of these transients depend on how many generators are operating and how much base load power they are supplying. This makes sense, as the energy stored in the inertia of the machines and the armature reactances of the machines vary with load. Each transient can be categorized as an "event type" based on the load action that caused it, the number of generators running prior to it, and the total base load prior to it. A few days of observation proved suitable for providing a full suite of transient exemplars for the base.

A. FREQUENCY SIGNATURES

ECU heaters are the largest loads at the BCIL [19] and create larger frequency deviations than all other loads except the latrine pump. Fig. 4 shows the maximum frequency

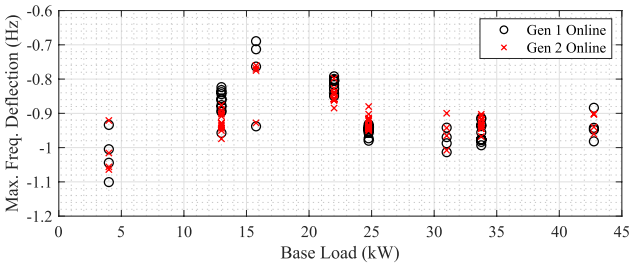

FIGURE 4. With only one generator powering the BCIL microgrid, ECU turn-on events triggered frequency transients ranging in magnitude between approximately 0.65Hz and 1.1Hz depending on the base load.

deflection as a function of base load for all ECU turn-on events with a single generator powering the grid. The figure reveals a moderate dependency between the size of the frequency transients and the base load at the time of the ECU event. A plot of ECU turn-off event maximum frequency deflections looks similar in shape, but reflected about the x-axis (as the turn-on and turn-off are essentially mirror images) and shifted out approximately 10kW as events are categorized by the base camp draw leading up to each event.

ECU transients take on one of two distinct shapes when only one generator is running. Fig. 5 plots each ECU turn-on transient with a camp base load of approximately 13kW. Here, the faint lines are the individual transients, and the black line is a time-averaged composite waveform or ''exemplar''. Most transients look like the exemplar on the left, where the frequency deviation is arrested and brought smoothly back to its nominal value over the course of 1.5 seconds. Occasionally, the frequency is arrested and ''aggressively'' brought back near its nominal value in less than 0.5 seconds, as shown on the right. ECU turn-off events create similar transients, but opposite in sign. These differing behaviors may be a result of time-varying and/or nonlinear control in the generators' frequency regulators.

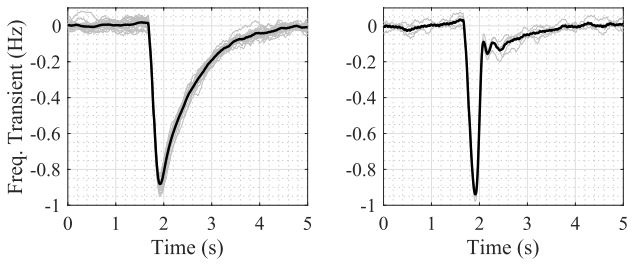

FIGURE 5. Both ''slow'' and ''fast'' transients were observed for ECU turn-on events at some load levels.

With both generators operating in parallel, the peak frequency deviation of an ECU turn-on or turn-off transient is generally smaller. In this case, base load variations become more significant, as illustrated in Fig. 6. A single transient exemplar similar to the left plot in Fig. 5 represents these transients.

Generator turn-on events were not found to create significant frequency transients, with maximum frequency deflections smaller than 200mHz regardless the base load.

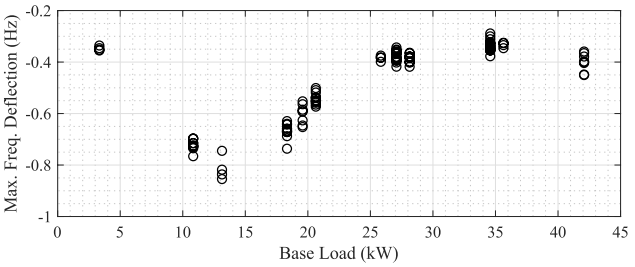

FIGURE 6. When both generators power the BCIL microgrid, the ECU turn-on event related frequency transients varied more significantly with base load than when only one generator is powering the microgrid.

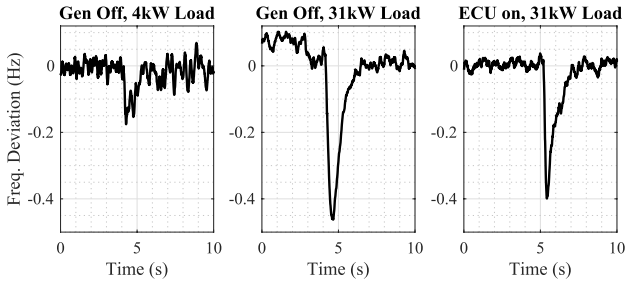

FIGURE 7. The frequency transient produced by a generator turn-off event. Note that at low base loads the transient is nearly undetectable, and that the ECU turn-on frequency transient closely resembles that of a generator turn-off around a base load of 25% of the generation capacity of two generators (30kW).

Generator turn-off events, however, did induce significant frequency transients at larger base loads, but not at smaller ones. Fig. 7 depicts example frequency deviations for base loads of 4kW (left) and 31kW (middle). At low loads, the transient is small and difficult to identify. However, at higher loads, generator turn-off events produce easily detected frequency transients. These transients closely resemble those induced by some ECU turn-on events when two generators are operating, e.g., the ECU turn-on event shown on the right in Fig. 7. Similarly, latrine pump turn-on events produce frequency transients easily confused with some ECU turn-on events, even though the pump consumes less than half the steady-state power of an ECU heater. However, due to its sizable inrush current, it still creates a frequency deviation of comparable size as shown in Fig. 8. The pump was the only

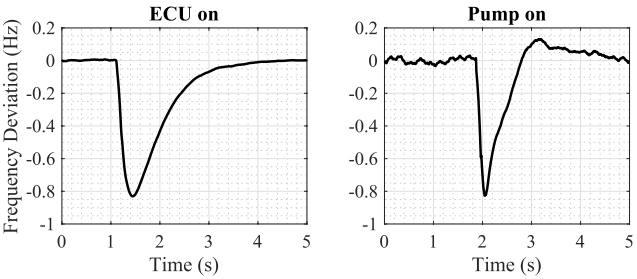

FIGURE 8. The large inrush current of a latrine pump turn-on event makes its transient difficult to distinguish from that of some ECU turn-on events, despite the fact that it is a less powerful load. These similar-looking transients were captured with one generator running under a base load between 21kW and 24kW.

load on the BCIL grid found to create transients comparable to the ECUs.

Frequency transients as event signatures cannot, on their own, provide unambiguous indication of each electrical event type on the BCIL microgrid. While frequency transients provide strong indications of all ECU event types, under some conditions ECU turn-on event signatures can be very similar to generator turn-off events or latrine pump turn-on events. Further, the frequency signatures corresponding to generator turn-on events and those corresponding to generator turn-off events under low base loads are weak indicators of these events. Therefore, at least one additional event signature stream must be observed for unambiguous electrical event monitoring at BCIL.

B. SEVENTH-HARMONIC VOLTAGE TRANSIENTS

The in-phase seventh-harmonic voltage content, i.e., $\hat{V}_{7,r}[m] = \Re\{\hat{V}_7[m]\}$, proved particularly useful for resolving the ambiguities associated with the frequency transients. Examining both streams (frequency and seventh-harmonic voltage) together permits unambiguous electrical event identification at BCIL. More generally, some combination of harmonic and frequency streams is likely to provide unique identification of key loads on many microgrids, and leads to an interesting and useful machine learning problem for load identification from voltage waveform transients.

Fig. 9 presents an approximate seventh-harmonic circuit model for the microgrid of Fig. 2 that is useful for understanding the effects of electrical events on the grid's seventh-harmonic content. Here, line impedances are ignored as we found load and generator turn-on and turn-off events to be reasonably uniform across all measurement points. Variable resistor R_{lb} represents the controllable load bank, and all ECU heater impedances and seventh-harmonic current injections are lumped into R_h and $I_{v,7}$, respectively. Source $I_{v,7}$ in the model is the sum of all the ECU ventilation fan seventh-harmonic currents, and R_h varies with the number of energized ECU heaters such that,

$$R_h = \left(\frac{s_1}{R_{h1}} + \frac{s_2}{R_{h2}} + \frac{s_3}{R_{h3}} + \frac{s_4}{R_{h4}}\right)^{-1}. \tag{6}$$

Here, s_n is a binary variable equal to one when the n^{th} ECU heater is energized and zero when it is not.

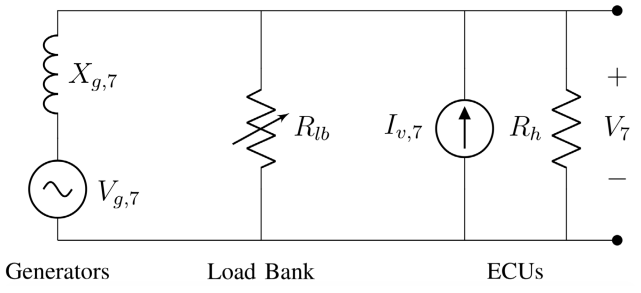

FIGURE 9. Equivalent seventh-harmonic circuit model of the BCIL test setup.

Source $V_{g,7}$ in the model represents the combined seventh-harmonic voltage of the two generators, and $X_{g,7}$ represents their combined reactance at 420Hz (seventh harmonic of 60Hz). With the two generators essentially identical, their combined source characteristics can be described as

$$V_{g,7}(P_L, n_g) = V_{g1,7}\left(\frac{P_L}{n_g P_{g,r}}\right) \tag{7}$$

and

$$X_{g,7}(n_g) = \frac{X_{g1,7}}{n_g}. \tag{8}$$

Here, $V_{g1,7}(\gamma)$ is the seventh-harmonic voltage of a single generator under the per generator normalized load (percent capacity),

$$\gamma = \frac{P_L}{n_g P_{g,r}}, \tag{9}$$

where P_L is the total fundamental power provided to the grid by n_g generators each with a capacity rating of $P_{g,r}$ (60kW). Similarly, $X_{g1,7}$ is the output reactance of a single generator.

The combined contribution of these two bulk sources to the seventh-harmonic voltage observed at each heater is

$$V_7 = \left(\frac{R_{lb} \parallel R_h}{jX_{g,7} + R_{lb} \parallel R_h}\right) V_{g,7} + \left(R_{lb} \parallel R_h \parallel jX_{g,7}\right) I_{v,7}, \tag{10}$$

where the $\parallel$ operator indicates the parallel combination of two impedances. At the BCIL, $X_{g,7} \ll R_{lb} \parallel R_h$. This is likely to also be true for most practical grids, as generator reactances at 60Hz need to be negligible to avoid significant voltage droop in the system. Therefore, the seventh-harmonic voltage at each heater can be approximated as

$$V_7 \approx V_{g,7} + jX_{g,7}I_{v,7}. \tag{11}$$

That is, the seventh-harmonic voltage measurements at each ECU depend on both the seventh-harmonic voltage distortion of the generators and the seventh-harmonic currents injected by the three-phase rectifiers of the ECU ventilation fans. Notably, $X_{g,7}$ does not significantly affect the generators' seventh-harmonic voltage distortion contributions. Further, $V_{g,7}$ is a function of normalized load when combining (7) and (9). These relationships were confirmed through steady-state tests with all ECU ventilation fans off so as to eliminate the contribution of $I_{v,7}$. Fig. 10 plots $\hat{V}_{7,r}$, which was found to be a monotonically increasing function of the normalized load, γ. Both generators produce similar levels of seventh harmonic distortion, as does their parallel combination, even though $X_{g,7}$ decreases when the two are paralleled.

When the ventilation fans are operating, their seventh-harmonic currents $I_{v,7}$ interact with the generator reactances to shift the in-phase seventh-harmonic voltages measured at the ECUs as shown in Fig. 11. Here, all data points from Fig. 10 are repeated for reference. This shift is more pronounced when only one generator is operating, as $X_{g,7}$ is twice as large compared to when both generators operate

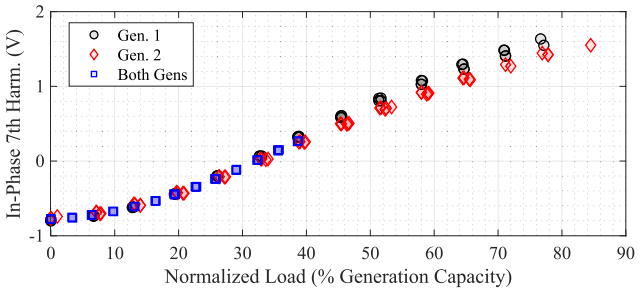

FIGURE 10. In-phase seventh-harmonic voltage measured at the ECUs when no ECU ventilation fans are operating.

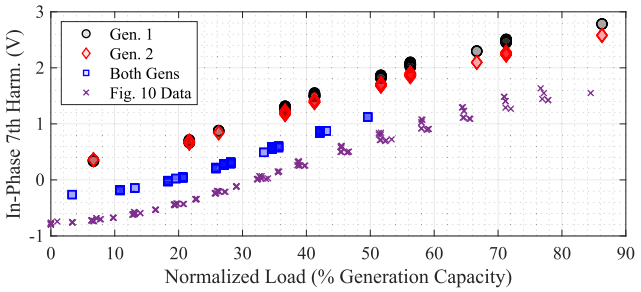

FIGURE 11. In-phase seventh-harmonic voltage measured at the ECUs when the ECU ventilation fans are operating. These variable speed drive fans impart seventh-harmonic currents which combine with the generator reactances to shift seventh-harmonic voltages measured at the ECUs.

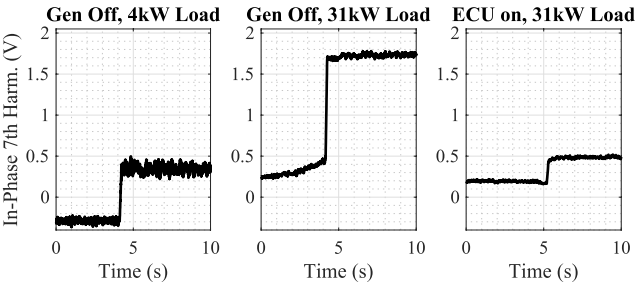

FIGURE 12. P7 data gathered under generator operation loaded by the load bank and ECUs. The current injected by the ECU ventilation fans was observed to create significant additional seventh-harmonic voltage in the circuit.

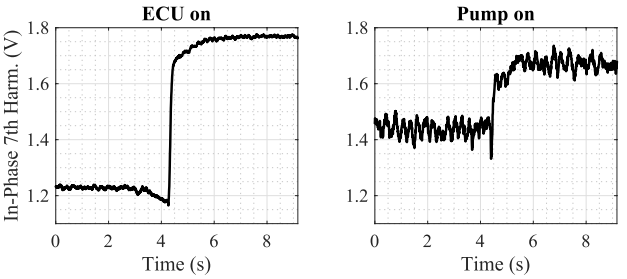

FIGURE 13. The delta-connected power electronic rectifier in the ECU creates a distinctively large turn-on transient in P7.

(assuming the generators are identical). The ventilation needs of each tent dictate fan speed and vary with time. This variation is created by a power electronic controller that creates seventh-harmonic currents. Therefore, the $I_{v,7}$ contribution to V_7 is not necessarily constant. However, these variations generally occur slowly compared to the abrupt changes in $V_{g,7}$ accompanying the steps in P_L caused by a load turn-on or turn-off event.

This seventh-harmonic voltage relationship with normalized load resolves the ambiguities left over from the frequency signatures. Specifically, generator turn-on events (n_g increases by one), which create relatively small frequency transients, generate large step-down transients in $\hat{V}_{7,r}$ due to the corresponding decreases in $X_{g,7}$ and γ ((8) and (9), respectively). In Fig. 11, this transient associated with a second generator activation manifests as both a shift down from a single generator curve to the two-generator curve and a shift left in normalized load, further decreasing the in-phase seventh-harmonic voltage.

Conversely, generator turn-off events generate large step-up transients in $\hat{V}_{7,r}$. Fig. 12 provides example $\hat{V}_{7,r}$ signatures corresponding to the same generator turn-off events of Fig. 7. Notably, the voltage transient on the left corresponding to a generator turn-off at low load provides a clear event signature, whereas the frequency transient did not. Further, the size of the $\hat{V}_{7,r}$ generator turn-off transient in the middle plot is easily distinguishable from the ECU turn-on event transient of the right plot, while the two corresponding frequency transients are easily confused. Similarly, Fig. 13 reveals that the $\hat{V}_{7,r}$ steps corresponding to the frequency transients of Fig. 8 help to distinguish between an ECU turn-on and pump turn-on, as the size of these steps is dictated by the steady-state power demand of the loads rather than the in-rush power.

V. TOOLS FOR SIGNATURE IDENTIFICATION

When considered together, frequency and in-phase seventh-harmonic voltage streams provide detectable and distinct transients that indicate four important microgrid events: ECU heater on, ECU heater off, Generator on, and Generator off. Fully deployable identification systems might require machine learning techniques for event detection and identification, e.g., the neural networks used in NILM applications [20]. More data might be needed as the model structure increases in complexity [21]. Our data set collected at BCIL was well analyzed with an approach, derived from convolutional neural networks (CNN), to create an ad hoc correlation-based transient identification algorithm using "fingerprint" exemplars, i.e. representative transient signatures, to identify events. Other classification schemes could also serve as a transient pattern identifier.

A. EXEMPLAR CREATION

To generate signature exemplars, we manually labeled a set of 512 ECU events and 15 generator events, each consisting of 1601 m-samples (approx. 13.3s) of frequency and 7th-harmonic data containing each stream's transient. From this set of labeled data, we selected 268 ECU events and 11 generator events to create event exemplars from similarly

shaped transients in this training set. Remaining data served as test sets for cross-validation. Creating these exemplars allowed the use of correlation methods for transient identification. This approach also minimizes the number of exemplar waveforms that must be saved by a local ECU controller, easing local requiremens on data storage and analysis in real-time.

Fig. 14 illustrates the exemplar formulation process. The exemplar creation algorithm receives a transient signature set with labeled events indicating the cause of the transient, the number of dispatched generators leading up to the event, and the base load just before the event. For each of the two streams that comprise the transient signature, the algorithm assesses whether the transient matches with any previously generated exemplar for that event type, number of generators, and base load. This matching is conducted by first aligning the transient signature, $y[m]$, with the exemplar, $x[m]$, by index-shifting the transient by l_o indices where,

$$l_o = \underset{l}{\text{argmax}} \sum x[m]y[m+l]. \tag{12}$$

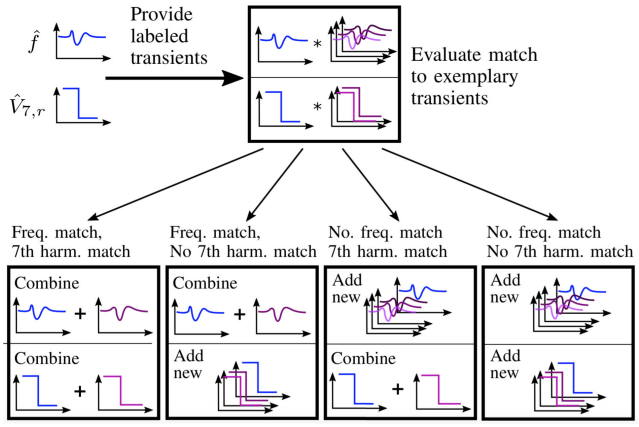

FIGURE 14. The exemplar management algorithm compares a transient labeled with event type and base load to all transients in the corresponding exemplar for each stream. The measured transient will either update an existing exemplary transient (+ sign) or be added as a new one.

Here, l_o is the lag corresponding to the maximum in the cross-correlation of the two waveforms. The match is then scored as

$$S = \frac{\sum (x[m] - y[m+l_o])^2}{\sum x\,[m]^2}, \tag{13}$$

i.e., the squared "distance" between the transient candidate and the exemplar normalized to the energy of the exemplar.

The lower the value of S, the better the match between the two signals. As such, a threshold level for matching was determined empirically. For all seventh-harmonic transients corresponding to any event type, and all frequency transients corresponding to ECU on-events and both ECU and generator off-events, this threshold was set to $S_o = 0.2$. For generator turn-on events, where the frequency transients are less distinct, this threshold was $S_o = 0.45$. If the algorithm determines that the transient matches an exemplar, it recursively updates the exemplar as,

$$x[m] = \alpha x[m] + (1-\alpha)\, y[m+l_o]. \tag{14}$$

For this study, we set the recursive update factor, α, to 0.8.

The frequency and harmonics streams for each event are evaluated independently. Therefore, they can both match their exemplar and be combined as illustrated in the bottom left of Fig. 14, or one can match and be combined (bottom middle), or neither might match (bottom right). When a transient does not match a previous exemplar or no previous exemplar exists, the algorithm sets the transient as a new exemplar. Some events, e.g., a generator turn-off under low loading (Fig. 7), do not create significant transients in the frequency stream. For these events, only the seventh-harmonic transient is used in exemplar creation. Using this technique reduces the number of total frequency and in-phase seventh-harmonic exemplars from 279 of each to 56 and 64, respectively. This can provide a useful savings in memory storage for each ECU load controller running an transient identifier.

B. ON-LINE TRANSIENT DETECTION

These exemplars permit transient identification by first detecting potential events in the frequency and seventh-harmonic streams and then matching new events to known exemplars. At BCIL, the rate of event generation and the homogeneity of the large ECU loads allows a change-of-mean detector to perform well as a transient detector, although other choices are possible. In the frequency stream the detector classifies a deviation exceeding 200mHz for more than 4ms, or by more than 10mHz for more than 2s, as a potential transient. These criteria were chosen based on the observed noise variance and the magnitudes of the frequency transients caused by events of interest.

In the seventh-harmonic stream, an edge corresponding to a step greater than 0.1V is considered a transient for the BCIL loads. To detect an edge, the transient detection algorithm smoothes the $\hat{V}_{7,r}[m]$ stream using a Gaussian low-pass filter with a standard deviation of 0.3s, and then evaluates the first difference of the result, $s[m]$, as,

$$d[m] = \frac{s[m] - s[m-1]}{t_z[m] - t_z[m-1]}. \tag{15}$$

A local maximum in $d[m]$ exceeding three times its standard deviation evaluated across the exemplar window is empirically set to indicate an edge. The identification algorithm then assesses the step size by averaging the values of $\hat{V}_{7,r}[m]$ for 1.5s before and after the detected edge, and classifies the step as a transient if the difference of these averages exceeds the 0.1V change in magnitude cutoff.

C. TRANSIENT IDENTIFICATION

Once an event has occurred, the identification algorithm compares the measured transient to all event exemplars corresponding to the estimated generator configuration and base load. This estimation is based on previously identified

transients and/or the level of $\hat{V}_{7,r}$ (Figs. 10 and 11). This matching algorithm, illustrated in Fig. 15, follows the same process as that used in exemplar creation and uses the same threshold values.

Measured transients are compared with the exemplar transients of each event type. As depicted in the ECU turn-on event category in the top left of Fig. 15, event types can contain multiple exemplars for one or both of the two streams. In these instances, the match score of the measured transient is calculated for each exemplar transient and the best score is taken. In the case of a generator turn-off under low loading conditions, there is no frequency exemplar to compare against, and the frequency transient score is instead determined as the scaled RMS value of its deviation,

$$S = \sqrt{\frac{\sum \Delta\hat{f}[m]^2}{E_o}} S_o. \tag{16}$$

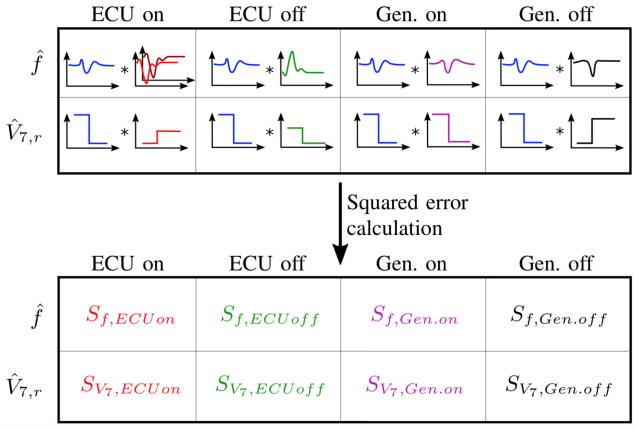

FIGURE 15. Overview of the transient-identification algorithm. The observed transients in both streams (colored blue, on the left of each cell) are compared with the exemplar transients for each event of interest.

Here, $E_o = 2.4$, which is the signal energy of a frequency deviation of 10mHz for 2 seconds (240 m-samples), i.e., the larger energy value of the frequency transient detection thresholds described in the transient detection section. S_o is set to 0.2, the matching threshold for generator turn-off frequency transients. If these match scores are below the threshold values for both the frequency and seventh-harmonic streams of a particular event type, the transient is identified as that event type. If no event is identified after this process, the detected transient is ignored.

D. "COLLISION" TRANSIENTS

Simultaneous or near-simultaneous events create "collision transients." Collision transients can be caused by the actions of any device, including ECUs, generators, or latrine pumps. They are not, in general, repeatable or distinct. The exact timing of the events that cause them have a large effect on the conglomerate shape and extent of the transient. Collision transients, while rare, are therefore currently unidentifiable. While reconciling these overlapping events is beyond the scope of this paper, we note its importance and point to two possibilities for maintaining situational awareness in the presence of collision transients. First, the "collision" may be resolvable as the sum of known exemplars. Second, it may not be necessary to resolve the exact details of the collision. For an autonomous ECU control algorithm, it may be sufficient to know that a collision has occurred, and develop a set of operating rules for resolving and moving past the collision with individual control efforts, as discussed in [10].

VI. ALGORITHM DEMONSTRATION

To demonstrate the functionality of the nonintrusive voltage monitoring algorithm, the exemplar formation and transient identification algorithms described in the previous section were applied to the field data containing all 512 ECU events, 15 generator events, and several events corresponding to other loads on the grid, e.g. the latrine pump. These events include those used to create the exemplars and also the cross-validation data set. During this process, the transient identification algorithm maintained an estimate of the total base load and the number of operating generators by identifying the transients associated with changes to those parameters. The identification algorithm correctly identified all 527 recorded transient. Examples of this event tracking are provided in Figs. 16-18, where the tallied events are provided in the top plots and the frequency and in-phase seventh-harmonic streams are provided in the middle and bottom plots, respectively.

In Fig. 16, the transient identifier correctly distinguishes the generator turn-off event at 189.2 mins and then a series of ECU on and off transients occuring between 190.9 and 193.7 mins. Notably, the identifier ignores the event occurring at 190.3 mins. At this moment, all ECUs cycled simultaneously to fully "off," causing the ventilation fans to turn off. This in turn caused the abrupt drop in seventh harmonic and the small frequency transient. At approximately 190.75 mins, we restarted the ECU ventilation fans, which resulted in the ramp up in seventh harmonic as the variable speed driven

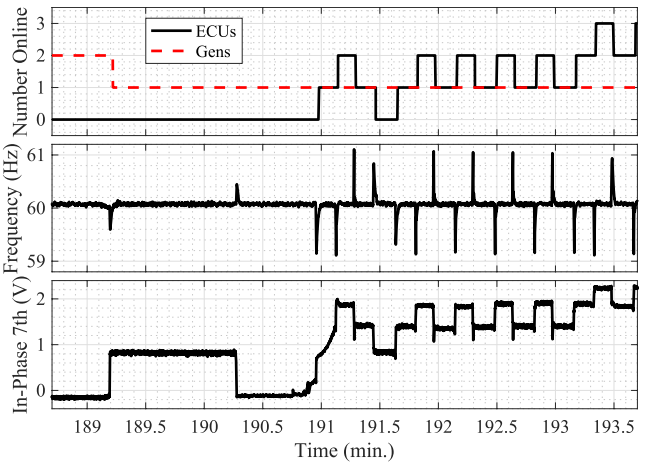

FIGURE 16. Transient-based detection of a generator turn-off event followed by a series of ECU turn-on and off events at the BCIL.

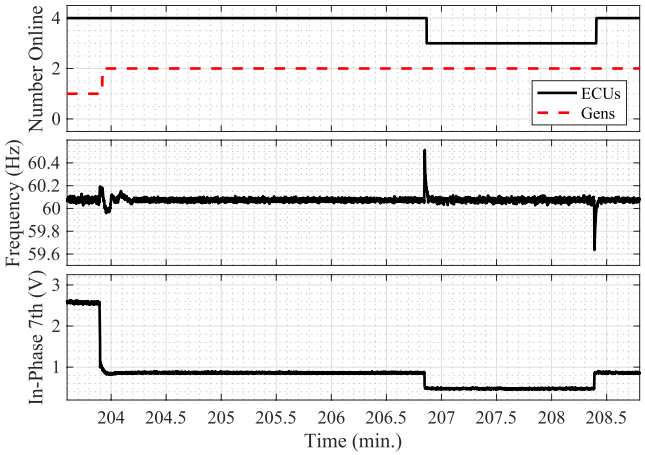

FIGURE 17. Transient-based detection of a generator turn-on event followed later by a single ECU turn-on event and single ECU turn-off events.

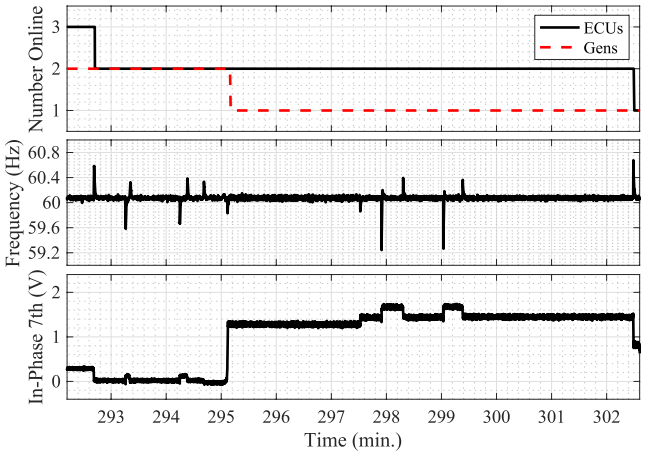

FIGURE 18. Transient-based detection of ECU and generator events, while simultaneously ignoring latrine pump events.

fans return to rated speeds. Even though the first ECU turn-on event occurs in the middle of this ramp up (190.95 mins), the algorithm is still able to identify this event.

Fig. 17 demonstrates the ability of the algorithm to correctly identify a generator turn-on event, characterized by the small frequency disruption but large seventh-harmonic step at approximately 203.9 mins. Two ECU events follow a few minutes later. Finally, Fig. 18 provides examples of the algorithm ignoring a series of latrine pump events. Following an ECU turn-off event at 292.75 mins while two generators were online, the latrine pump cycled on and off twice, first at 293.2 mins and then later at 294.2 mins. Later, after an identified generator turn-off event at 295.2 mins, the latrine pump again cycles twice, first at 297.9 mins and then at 299 mins. A few minutes later, the algorithm correctly detects the final ECU turn-off event.

VII. CONCLUSION

Most nonintrusive monitors, and power meters in general, measure both current and voltage. This paper has demonstrated an effective application of a nonintrusive monitor that can detect significant events and identify them strictly from changes in the voltage waveform of the utility. Voltage-only load identification means that any load on a local utility network can, in principle, identify the operating schedule of substantial loads in the network neighborhood. No current sensors are necessary, and the utility itself effectively doubles as a load-monitoring information exchange network. The scheme could also be augmented or enhanced, where appropriate, with other signals, including power-line carrier signals, to confirm or ensure the detection of load operation.

Grids or sections of power grids may be resource constrained for different reasons [22], [23]. True microgrids on land, such as the US Army FOBs, or elsewhere, e.g., on ships or aircraft, are constrained by generation resources. These constraints include absolute power limits and also a desire for efficient operation. Sections of other grids may be effectively constrained by distribution components like transformers. This paper has demonstrated techniques that allow an individual load to recognize and react to the operation of other loads on the local grid. This information could be used by ''aware'' loads to self-schedule their operation to avoid power demand peaks. In much the same way that a self-driving vehicle can share a road with different owners operating with different goals, this ''aware'' approach to load operation permits loads to share the grid while minimizing peak demand without conflict or invasive networking requirements.

ACKNOWLEDGEMENT

The authors would like to express their thanks for the support and skill of the staff at the U.S. Army Base Camp Integration Laboratory, especially William Singleton. They would also like to thank Jacob Jurewicz for his advice and insight.

REFERENCES

[1] S. C. Shabshab, J. K. Nowocin, P. Lindahl, and S. B. Leeb, ''Microgrid modeling and fuel savings opportunities through direct load control,'' in *Proc. IEEE IES IECON*, Oct. 2018, pp. 231–236.
[2] C. M. Colson and M. H. Nehrir, ''Comprehensive real-time microgrid power management and control with distributed agents,'' *IEEE Trans. Smart Grid*, vol. 4, no. 1, pp. 617–627, Mar. 2013.
[3] C. X. Dou and B. Liu, ''Multi-agent based hierarchical hybrid control for smart microgrid,'' *IEEE Trans. Smart Grid*, vol. 4, no. 2, pp. 771–778, Jun. 2013.
[4] M. H. Cintuglu, T. Youssef, and O. A. Mohammed, ''Development and application of a real-time testbed for multiagent system interoperability: A case study on hierarchical microgrid control,'' *IEEE Trans. Smart Grid*, vol. 9, no. 3, pp. 1759–1768, May 2018.
[5] X. Lu, W. Wang, and J. Ma, ''An empirical study of communication infrastructures towards the smart grid: Design, implementation, and evaluation,'' *IEEE Trans. Smart Grid*, vol. 4, no. 1, pp. 170–183, Mar. 2013.
[6] F. Salvadori, C. S. Gehrke, A. C. de Oliveira, M. de Campos, and P. S. Sausen, ''Smart grid infrastructure using a hybrid network architecture,'' *IEEE Trans. Smart Grid*, vol. 4, no. 3, pp. 1630–1639, Sep. 2013.
[7] Z. Huang, T. Zhu, H. Lu, and W. Gao, ''Accurate power quality monitoring in microgrids,'' in *Proc. 15th ACM/IEEE Int. Conf. Inf. Process. Sensor Netw.*, Apr. 2016, pp. 1–6.
[8] G. Ding, S. Zhang, J. Shan, F. Gao, and X. Gu, ''Autonomous control of active power electronics loads for frequency control of islanded microgrid,'' in *Proc. IEEE Energy Convers. Congr. Expo.*, Oct. 2017, pp. 1582–1587.
[9] J. Merino, P. Mendoza-Araya, G. Venkataramanan, and M. Baysal, ''Islanding detection in microgrids using harmonic signatures,'' *IEEE Trans. Power Del.*, vol. 30, no. 5, pp. 2102–2109, Oct. 2015.

[10] S. Shabshab, "Fuel-conserving environmental control strategies for small islanded microgrids," M.S. thesis, Dept. Mech. Eng., Massachusetts Inst. Technol., Cambridge, MA, USA, Jun. 2018.
[11] J. S. Donnal, J. Paris, and S. B. Leeb, "Energy applications for an energy box," *IEEE Internet Things J.*, vol. 3, no. 5, pp. 787–795, Oct. 2016.
[12] R. Cox, S. B. Leeb, S. R. Shaw, and L. K. Norford, "Transient event detection for nonintrusive load monitoring and demand side management using voltage distortion," in *Proc. Annu. IEEE Appl. Power Electron. Conf. Expo. (APEC)*, Mar. 2006, pp. 1–7.
[13] S. R. Shaw, C. R. Laughman, S. B. Leeb, and R. F. Lepard, "A power quality prediction system," *IEEE Trans. Ind. Electron.*, vol. 47, no. 3, pp. 511–517, Jun. 2000.
[14] C. Laughman, K. Lee, R. Cox, S. Shaw, S. Leeb, L. Norford, and P. Armstrong, "Power signature analysis," *IEEE Power Energy Mag.*, vol. 1, no. 2, pp. 56–63, Mar./Apr. 2003.
[15] D. He, W. Lin, N. Liu, R. G. Harley, and T. G. Habetler, "Incorporating non-intrusive load monitoring into building level demand response," *IEEE Trans. Smart Grid*, vol. 4, no. 4, pp. 1870–1877, Dec. 2013.
[16] M. Dong, P. C. M. Meira, W. Xu, and C. Y. Chung, "Non-intrusive signature extraction for major residential loads," *IEEE Trans. Smart Grid*, vol. 4, no. 3, pp. 1421–1430, Sep. 2013.
[17] J. Paris, J. S. Donnal, Z. Remscrim, S. B. Leeb, and S. R. Shaw, "The sinefit spectral envelope preprocessor," *IEEE Sensors J.*, vol. 14, no. 12, pp. 4385–4394, Dec. 2014.
[18] W. Shanming, W. Xiangheng, S. Pengsheng, F. Yu, M. Weiming, and Z. Gaifan, "Research on voltage harmonic distortion of synchronous generators," in *Proc. 5th Int. Conf. Elect. Mach. Syst.*, vol. 1, Aug. 2001, pp. 400–403.
[19] M. Gillman, W. M. Singleton, R. A. Wilson, W. Cotta, J. Donnal, J. Paris, and S. Leeb, "Accounting for every kilowatt," *Defense AT L*, vol. 43, no. 5, pp. 44–49, Sep. 2014.
[20] D. Green, S. Shaw, P. Lindahl, T. Kane, J. Donnal, and S. Leeb, "A multiscale framework for nonintrusive load identification," *IEEE Trans. Ind. Informat.*, to be published.
[21] J. Kelly and W. Knottenbelt, "Neural NILM: Deep neural networks applied to energy disaggregation," in *Proc. 2nd ACM Int. Conf. Embedded Syst. Energy-Efficient Built Environ.*, 2015, pp. 55–64.
[22] S. Althaher, P. Mancarella, and J. Mutale, "Automated demand response from home energy management system under dynamic pricing and power and comfort constraints," *IEEE Trans. Smart Grid*, vol. 6, no. 4, pp. 1874–1883, Jul. 2015.
[23] C. Eksin, H. Deriç, and A. Ribeiro, "Demand response management in smart grids with heterogeneous consumer preferences," *IEEE Trans. Smart Grid*, vol. 6, no. 6, pp. 3082–3094, Nov. 2015.

SPENCER C. SHABSHAB received the master's degree in mechanical engineering from the Massachusetts Institute of Technology, in 2018. He is currently a Submarine Officer with the United States Navy.

PETER A. LINDAHL graduated the B.S. degree in electrical engineering from Penn State University, in 2003, and the M.S. degree in electrical engineering and the Ph.D. degree in engineering from Montana State University, in 2009 and 2013, respectively. He then joined the Research Laboratory of Electronics at the Massachusetts Institute of Technology, as a Postdoctoral Associate, in 2014. He is currently a Senior Associate with the Electrical Engineering & Computer Science Practice, Exponent, Inc., where he provides technical consulting services regarding energy and power system operation, power system and machinery diagnostics and condition monitoring, and root-cause failure analysis and safety evaluation of industrial equipment and consumer products.

J. KENDALL NOWOCIN received the Ph.D. degree from the Massachusetts Institute of Technology, in 2017. He has experience in developing small and large power systems ranging from 10-kW residential and 100-kW industrial electrical projects with Atlantic Electric LLC to a 2.4-GW power plant for a SC power utility. He is the CTO and the Co-Founder of CoolCrop, a social entrepreneurship startup in agriculture technology and microgrids.

STEVEN B. LEEB received the doctoral degree from the Massachusetts Institute of Technology, in 1993. He has been a member on the MIT Faculty in the Department of Electrical Engineering and Computer Science, since 1993. He also holds a joint appointment in MIT's Department of Mechanical Engineering. He is currently concerned with the development of signal processing algorithms for energy and real-time control applications.